Correlations and Entanglement of Microwave Photons Emitted in a Cascade Decay

Simone Gasparinetti,* Marek Pechal, Jean-Claude Besse, Mintu Mondal, Christopher Eichler, and Andreas Wallraff
Department of Physics, ETH Zurich, CH-8093 Zurich, Switzerland
(Received 2 June 2017; published 4 October 2017)

We use a three-level artificial atom in the ladder configuration as a source of correlated, single microwave photons of different frequency. The artificial atom, a transmon-type superconducting circuit, is driven at the two-photon transition between ground and second-excited state, and embedded into an on-chip switch that selectively routes different-frequency photons into different spatial modes. Under continuous driving, we measure power cross-correlations between the two modes and observe a crossover between strong antibunching and superbunching, typical of cascade decay, and an oscillatory pattern as the drive strength becomes comparable to the radiative decay rate. By preparing the source in a superposition state using an excitation pulse, we achieve deterministic generation of entangled photon pairs, as demonstrated by nonvanishing phase correlations and more generally by joint quantum state tomography of the two itinerant photonic modes.

DOI: 10.1103/PhysRevLett.119.140504

Single photons are expected to be key elements in the quantum internet [1], mediating interactions between its nodes and enabling entanglement distribution and quantum-state transfer protocols. They are also an indispensable resource in linear-optics quantum computing [2] and may find use in quantum metrology [3]. Sources of single photons and entangled photon pairs have been studied from the early days of quantum optics until our days [4,5]. In the last 15 years, the rise of superconducting circuits based on Josephson junctions in the context of quantum information processing [6], with transition frequencies in the microwave range, has given birth to the field of microwave quantum photonics [7]. In this domain, the exquisite degree of control achieved over individual artificial atoms (qubits) facilitates the generation of single photons by single-atom excitation and subsequent spontaneous emission into well-controlled, spatially confined transmission line modes [8–13]. Furthermore, real-time control of the emission rate [9–12] makes it possible to shape the temporal profile of the photon. The nonclassical properties of microwave radiation have been characterized using linear detectors [14–17], including single-photon antibunching [18,19], indistinguishability [20], and entanglement with the artificial atom used as the source [21]. Entanglement between two distinct microwave fields has also been shown in different settings [22–27].

Here we have studied the correlation properties of pairs of microwave photons emitted in the cascade decay of a superconducting artificial atom, coherently driven by two-photon resonant excitation. Atomic cascades played an important role as sources of polarization-entangled photons in the first Bell tests [28,29]. More recently, the biexciton cascade of a semiconductor quantum dot has been exploited to generate such photons deterministically and on a solid-state platform [30–34]. In a cascade decay, the photons are emitted sequentially, so their intensities are strongly correlated in time, as measured in a double-beam coincidence experiment [35,36]. Similar correlations can be found between the two sidebands of the resonance fluorescence triplet, due to cascade down a ladder of dressed states [37,38]. Recently, multiphoton correlations have also been observed in a strongly coupled atom-cavity system driven at a two-photon resonance [39]. All these experiments concentrate on *intensity* correlations; yet, perhaps less intuitively, the *phase* of photons emitted in cascade can also be correlated, provided (i) a single emitter is deterministically prepared into a superposition state, and (ii) the emitted radiation is detected in a phase-sensitive manner and with high efficiency. By meeting these requirements in our experiment, we highlight the intrinsically coherent nature of cascade decay and demonstrate a novel protocol to generate entanglement between itinerant field modes.

We have realized a photon source (Fig. 1) based on a transmon-type qubit [40,41], with two lowest transitions at $\omega_{ge}/2\pi = 7.0975$ GHz and $\omega_{ef}/2\pi = 6.8645$ GHz between the ground, $|g\rangle$, the first excited, $|e\rangle$, and the second excited state, $|f\rangle$, and a resulting anharmonicity $\alpha/2\pi = -233$ MHz. The transmon is driven via a weakly coupled input port [13,42] and decays into one of the two input ports of the single-pole, double-throw switch described in Ref. [42], with a measured rate $\Gamma_{ge}/2\pi = (1.94 \pm 0.02)$ MHz. The switch has a tunable center frequency, which we set to ω_{ge}, and a bandwidth of 150 MHz. Photons of frequency ω_{ge} (ω_{ef}) fall within (out of) the switch bandwidth and are routed from the source to output mode $\hat{e}$ ($\hat{f}$) [Fig. 1(a)]. Each output mode is amplified using a nearly quantum-limited Josephson parametric dimer (JPD) [43] and its two quadratures are measured by heterodyne detection. We characterize the scattering properties of the switch by driving it via its second input port [Fig. 1(d)]. On this basis, we estimate that

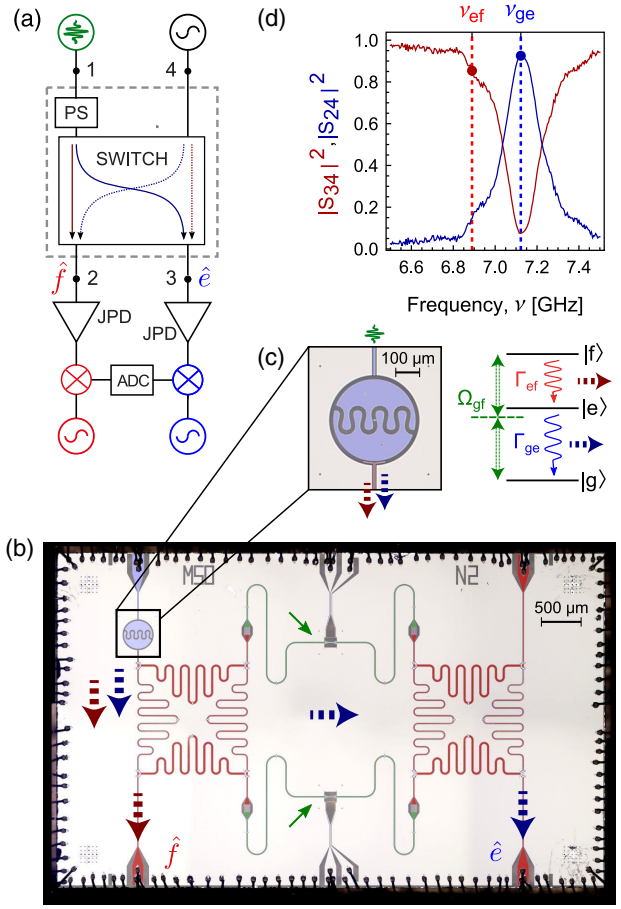

FIG. 1. Photon source and microwave switch. (a) Simplified scheme of the measurement setup. The photon source (PS) is coherently driven from input port 1. Input port 4 is used to characterize the scattering properties of the switch. The output modes $\hat{e}$ and $\hat{f}$ are amplified by Josephson parametric dimers (JPDs). The two quadratures of the amplified signals are measured by double heterodyne detection and recorded by an analog-to-digital converter (ADC). (b) False-color micrograph of the sample, illustrating the PS (blue) and the key components of the switch, two $\pi/2$ hybrid couplers (red) and two tunable resonators (green). (c) Closeup micrograph of the PS, a transmon asymmetrically coupled to input and output lines, and level scheme indicating the relevant transitions. The transmon is driven at the two-photon transition $\omega_{gf}/2$ with rate Ω_{gf} and decays by emitting photons at frequencies ω_{ef} and ω_{ge} and rates Γ_{ef} and Γ_{ge}, respectively. (d) Characterization of the switch via port 4: transmittance to ports 3 ($|S_{34}|^2$) and 2 ($|S_{24}|^2$) vs frequency ν. The transition frequencies of the transmon, ν_{ge} and ν_{ef}, are indicated by dashed lines.

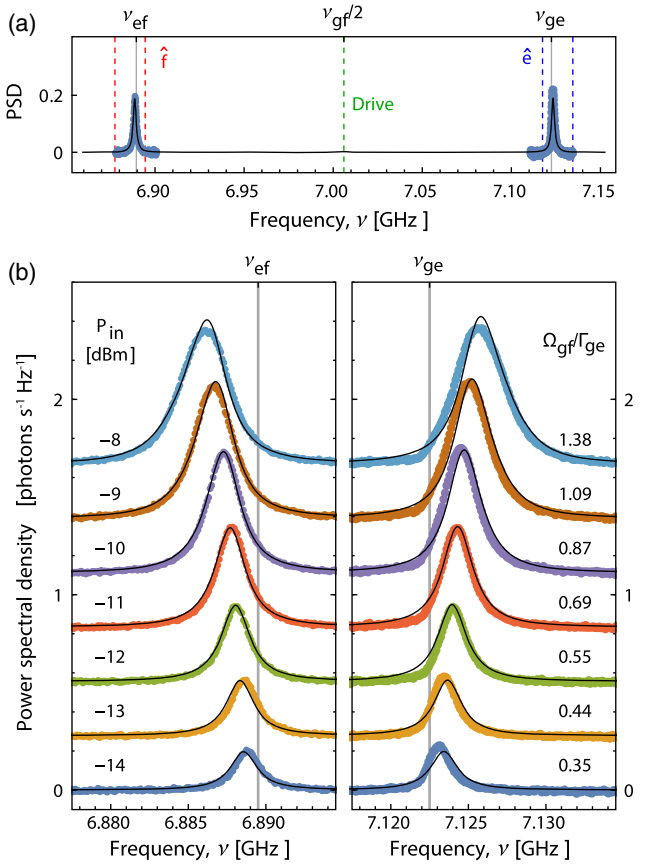

FIG. 2. Inelastic scattering under continuous excitation. (a) Power spectral density (PSD) of the radiation emitted by the source, driven at $\omega_{gf}/2$ and low power: theory (solid line) and combined measured traces (colored dots) from the two modes. (b) Measured power spectral densities in modes $\hat{f}$ (left) and $\hat{e}$ (right) for varying input powers, P_{in}. The traces are offset vertically for clarity and globally fitted to our model (solid lines), the only fit parameter being the total attenuation of the drive line (input 1 in Fig. 1). For each input power P_{in}, we note the corresponding $|g\rangle \leftrightarrow |f\rangle$ drive rate Ω_{gf}, relative to the decay rate Γ_{ge}.

our routing scheme has an efficiency of 92% (86%) for photons of frequency ω_{ge} (ω_{ef}).

We first investigate the cascade decay of our source under continuous-wave excitation. We coherently drive the two-photon transition between $|g\rangle$ and $|f\rangle$, with frequency $\omega_{gf}/2 = (\omega_{ge} + \omega_{ef})/2$ [level scheme in Fig. 1(c)]. We vary the input power P_{in} and analyze the spectrum of the scattered radiation (Fig. 2). Contributions from coherent (Rayleigh) scattering at the drive frequency are discarded in our detection chain. At low powers, the spectrum shows a single peak at each of the transition frequencies ω_{ge} and ω_{ef}. The photon flux into each mode, as given by the integrated power spectrum, first increases with power and then saturates as population is transferred into $|f\rangle$. At the same time, the two emission frequencies Stark-shift away from each other due to the driving of the two-photon transition [44]. The measured data are in excellent agreement with a model based on a Lindblad-type master equation and input-output theory (see Supplemental Material [45]). The Rabi frequency Ω_{gf} describing coherent oscillations between $|g\rangle$ and $|f\rangle$ is proportional to the drive strength *squared*, i.e., directly proportional to P_{in}, because we are driving a two-photon transition.

Further insight into the emitted radiation is provided by its statistical properties [14,17,18,20]. The power autocorrelation

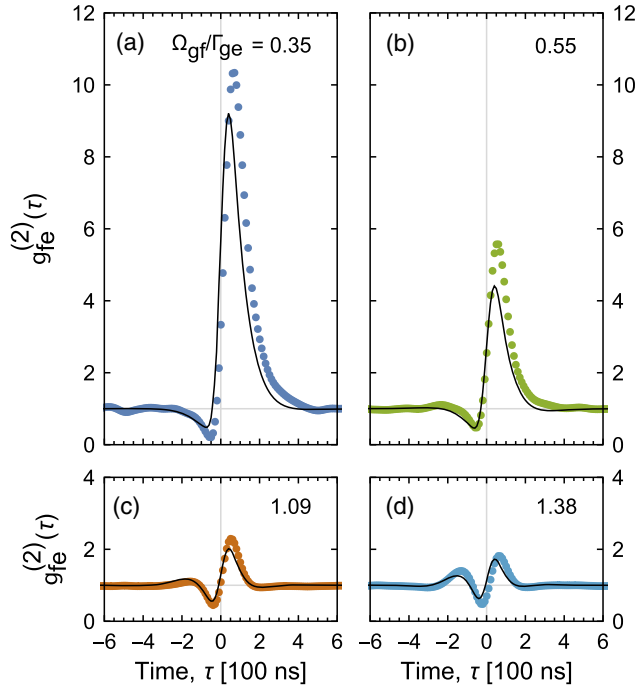

FIG. 3. Photon-photon correlations. Time-resolved power cross-correlation $g^{(2)}_{fe}(\tau)$ between modes $\hat{f}$ and $\hat{e}$, taken at the indicated, normalized drive rates Ω_{gf}/Γ_{ge} (dots). The solid lines are calculated based on the parameters of Fig. 2, taking into account the 10 MHz detection bandwidth of the used experimental setup and with no fit parameters.

functions of the two modes, $g^{(2)}_{ee}(\tau)$ and $g^{(2)}_{ff}(\tau)$, show that the emitted radiation is antibunched [45], a clear signature of single-photon emission [13,18,19]. Here, however, we focus on correlations *between* the two photons, as expressed by the normalized power cross-correlation function $g^{(2)}_{fe}(\tau) = \langle f^\dagger(0)e^\dagger(\tau)e(\tau)f(0)\rangle/(\langle e^\dagger e\rangle\langle f^\dagger f\rangle)$. A positive (negative) time delay τ corresponds to a photon being emitted in mode $\hat{e}$ after (before) a photon is emitted in mode $\hat{f}$. At the lowest drive powers [Figs. 3(a) and 3(b)], $g^{(2)}_{fe}(\tau)$ shows antibunching at negative time delays [$g^{(2)}_{fe}(\tau) \ll 1$] and strong superbunching at positive ones [$g^{(2)}_{fe}(\tau) \gg 1$], as expected for two time-correlated emissions occurring in a given sequence [35,36]. This pattern changes at higher powers [Figs. 3(c) and 3(d)], specifically, when the pump rate becomes comparable to the decay rates ($\Omega_{gf}/\Gamma_{ge} \approx 1$). Because of fast repopulation of the $|f\rangle$ level, there is an increased probability for the reverse sequence to occur, which results in a superbunching peak appearing at negative time delays. More generally, $g^{(2)}_{fe}(\tau)$ develops oscillations at frequency Ω_{gf}, revealing the coherent nature of the population transfer between $|g\rangle$ and $|f\rangle$. The observed properties are captured well by our model (solid lines), which has no free parameters [45].

To characterize the radiation emitted in a single cascade, we use a preparation pulse, whose time envelope is a

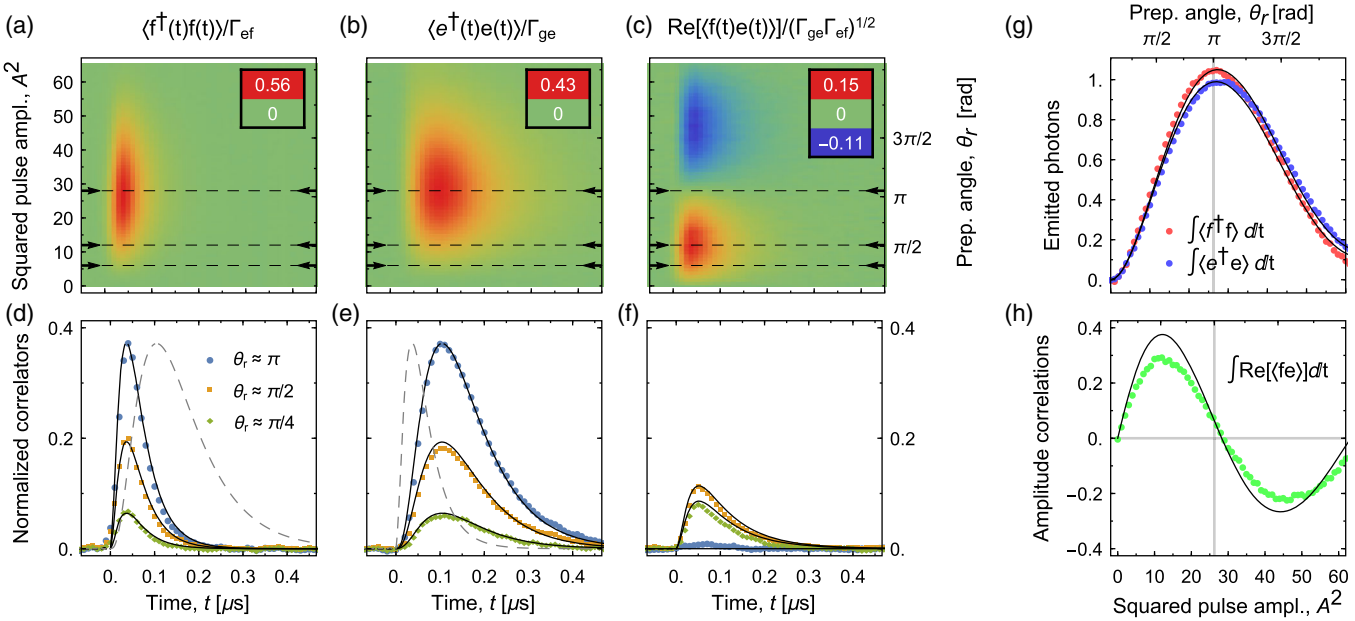

FIG. 4. Pulsed excitation: photon shapes and phase correlations. (a)–(c) Density plots of the normalized photon flux in each mode, $\langle f^\dagger(t)f(t)\rangle/\Gamma_{ef}$ (a) and $\langle e^\dagger(t)e(t)\rangle/\Gamma_{ge}$ (b), and of the real part of the normalized amplitude cross-correlation $\langle f(t)e(t)\rangle/(\Gamma_{ge}\Gamma_{ef})^{1/2}$ (c), vs time, t (horizontal axis), and squared amplitude of the excitation pulse, A^2 (left vertical axis). The right vertical axis shows the preparation angle θ_r, calibrated using the data of panel (g). (d)–(f) Data (colored dots) of (a)–(c) extracted along the dashed lines. Solid lines are calculations based on the measured parameters of the transmon, the preparation angle θ_r, and the measured bandwidth of each amplification chain. In (d),(e) we have also plotted a reference trace from the other panel (dashed lines). (g) Integrated photon fluxes, $\int\langle f^\dagger f\rangle dt$ and $\int\langle e^\dagger e\rangle dt$, vs A^2. The solid lines are a fit to the theory model, serving as a calibration for the preparation angle θ_r. (h) Integrated amplitude cross correlation, $\int\langle fe\rangle dt$, vs A^2: data (dots) and corresponding theory (solid line) for the same parameters as in (g).

truncated Gaussian of variance $\sigma = 5$ ns and controlled amplitude A. The pulse drives coherent oscillations between $|g\rangle$ and $|f\rangle$, ideally preparing the transmon in the state $\cos(\theta_r/2)|g\rangle + \sin(\theta_r/2)|f\rangle$, where θ_r is the preparation angle. The optimal pulse duration is determined by a tradeoff between decay during state preparation and spectral overlap with the neighboring transitions at ω_{ge} and ω_{ef}, which are direct single-photon transitions. We monitor the emitted radiation by performing ensemble averaging on the relevant moments of $e(t)$ and $f(t)$ [14,17].

We first consider the photon fluxes $\langle f^\dagger(t)f(t)\rangle$ and $\langle e^\dagger(t)e(t)\rangle$, whose time dependence corresponds to the temporal shapes of the emitted photons [Figs. 4(a),(d) and 4(b),(e)]. The two shapes differ from each other: the photon flux in the $\hat{f}$ mode reaches its maximum at an earlier time and decays faster than in the $\hat{e}$ mode. These features are explained by considering that (i) the decay rates into the two modes are different by a factor $\Gamma_{ef}/\Gamma_{ge} \approx 2$, due to the dipole matrix elements of the transmon [41], and (ii) while the $|f\rangle$ state is directly populated by the excitation pulse, the $|e\rangle$ state is initially empty: the two photons decay sequentially. The integrated photon fluxes, proportional to the photon numbers in each mode, oscillate as a function of the pulse amplitude squared [Fig. 4(g)]. These oscillations reflect those in the prepared f-state population, to which both photon numbers are proportional. We fit our data to a master equation simulation taking into account the time dependence of the preparation pulse as well as radiative decay during preparation [Fig. 4(g), solid lines], and use the fit to determine the preparation angle θ_r as a function of the pulse amplitude A.

We next consider the relative phase between the two photons. The amplitude-amplitude correlation $\langle f(t)e(t)\rangle$ is generally nonzero, indicating a well-defined relative phase [Figs. 4(c), 4(f), and 4(h)]. The correlation is largest when the source is prepared in an equal state superposition ($\theta_r = \pi/2, 3\pi/2$), and smallest when it is prepared in an energy eigenstate ($\theta_r = 0, \pi$). By contrast, we have verified that the individual mode amplitudes $\langle f(t)\rangle$ and $\langle e(t)\rangle$ vanish identically, regardless of the pulse amplitude. We interpret the observed results in terms of a mapping of the transmon state into two itinerant photonic modes, $\hat{e}$ and $\hat{f}$. These modes are defined (and measured) by integrating the signals $e(t)$ and $f(t)$ over weighted time windows corresponding to the temporal shape of the emitted photons (temporal mode matching) [15]. In a Hilbert space comprising the transmon as well as the two modes, the cascade decay is described by the transformation

$$\begin{aligned}&[\cos(\theta_r/2)|g\rangle + \sin(\theta_r/2)|f\rangle] \otimes |0_f\rangle \otimes |0_e\rangle \\ &\quad \rightarrow \cos(\theta_r/2)|g\rangle \otimes |0_f\rangle \otimes |0_e\rangle + \sin(\theta_r/2)|e\rangle \otimes |1_f\rangle \otimes |0_e\rangle \\ &\quad \rightarrow |g\rangle \otimes [\cos(\theta_r/2)|0_f\rangle \otimes |0_e\rangle + \sin(\theta_r/2)|1_f\rangle \otimes |1_e\rangle] \end{aligned} \quad (1)$$

where $|0_{f,e}\rangle$ and $|1_{f,e}\rangle$ indicate Fock states of the two modes with photon numbers zero and one. Equation (1) stands for an entangling operation in which the superposition state created in the transmon is eventually shared by the two modes.

We fully characterize the two modes by performing joint tomography on them [15,17] for the preparation angles $\theta_r = \pi$ and $\pi/2$ [Figs. 5(a) and (b)]. To do so, we integrate the two output signals with appropriate mode-matching filters [45]. The measured moments are referred to the two outputs of the switch using the calibration procedure described in the Supplemental Material [45]. The vanishing of first-order moments in Figs. 5(a) and 5(b) indicates that

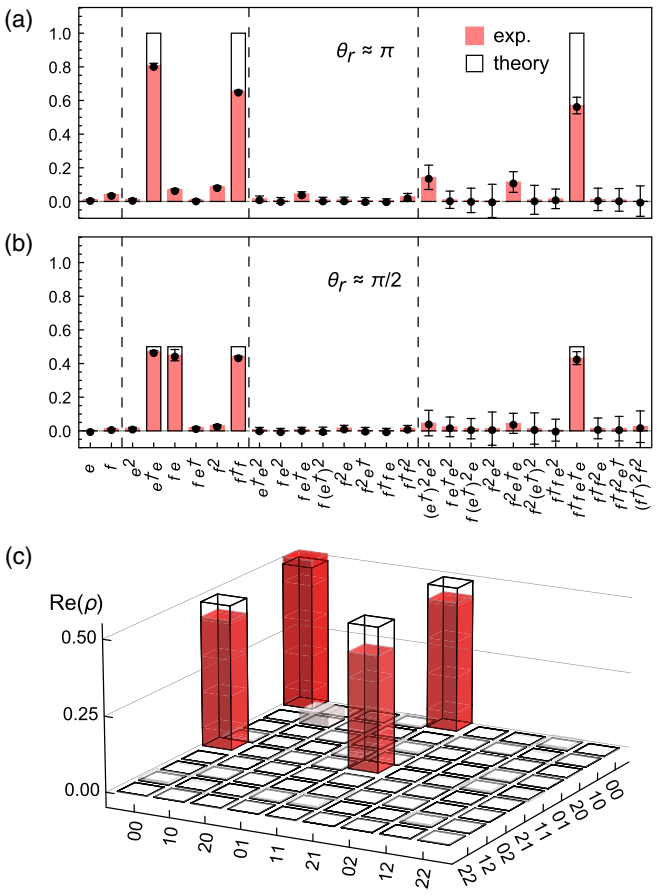

FIG. 5. Joint quantum state tomography of the modes $\hat{e}$ and $\hat{f}$. (a),(b) Reconstructed moments of the temporally matched modes $\hat{f}$ and $\hat{e}$ (absolute values) up to fourth order for the preparation angles (a) $\theta_r \approx \pi$ and (b) $\theta_r \approx \pi/2$ (color bars). The moments are referenced to the output of the switch. The expected moments for the states $|11\rangle$ and $(|00\rangle + |11\rangle)/\sqrt{2}$ are shown as wire frames in (a) and (b), respectively. (c) Real part of the most likely density matrix corresponding to the measured moments in (b), displaying a 91% fidelity to the state $(|00\rangle + |11\rangle)/\sqrt{2}$ (wire frames) and a negativity of −0.43. All entries of the imaginary part (not shown) have absolute value below 0.01.

the radiation in each mode has no definite phase. Photon-photon phase correlations manifest themselves in the amplitude correlation, $\langle \hat{f}\,\hat{e}\rangle$, which is substantial for a $\pi/2$ pulse and vanishes for a π pulse. The single-photon nature of the radiation is confirmed by the vanishing of the fourth-order moments, $\langle(\hat{f}^\dagger)^2\hat{f}^2\rangle$ and $\langle(\hat{e}^\dagger)^2\hat{e}^2\rangle$. Given the measured values for the moments and their respective standard deviations, we also determine the most likely density matrix ρ_{ML} describing the two modes at the output of the switch [17,20,49], having restricted the Hilbert space to up to two photons in each mode. For a $\pi/2$ pulse [Fig. 5(c)], we obtain a fidelity $F = \langle\psi|\rho_{\mathrm{ML}}|\psi\rangle = 91\%$ to the Bell state $|\psi\rangle = (|00\rangle + |11\rangle)/\sqrt{2}$, and a negativity $\mathcal{N}(\rho_{\mathrm{ML}}) = -0.43$.

In summary, our work demonstrates that in spite of its sequential nature, cascade decay must be regarded as a fully coherent process generating phase coherence between the emitted photons. Our excitation scheme can be extended to other architectures and generalized to multiphoton cascades and multiple modes. The ability to generate entanglement between spatially separated, itinerant radiation fields [20,22,24–27], as demonstrated in our experiment, is essential to quantum information distribution protocols.

We are grateful to Barry Sanders and Howard Carmichael for useful discussions and to Robin Buijs and Bradley Mitchell for technical assistance at an early stage of this project. This work is supported by the National Centre of Competence in Research "Quantum Science and Technology" (NCCR QSIT), a research instrument of the Swiss National Science Foundation (SNSF), and by ETH Zurich.

*simone.gasparinetti@phys.ethz.ch

[1] H. J. Kimble, Nature (London) **453**, 1023 (2008).
[2] E. Knill, R. Laflamme, and G. J. Milburn, Nature (London) **409**, 46 (2001).
[3] V. Giovannetti, S. Lloyd, and L. Maccone, Nat. Photonics **5**, 222 (2011).
[4] B. Lounis and M. Orrit, Rep. Prog. Phys. **68**, 1129 (2005).
[5] M. D. Eisaman, J. Fan, A. Migdall, and S. V. Polyakov, Rev. Sci. Instrum. **82**, 071101 (2011).
[6] M. Devoret and R. J. Schoelkopf, Science **339**, 1169 (2013).
[7] B. Fan, G. J. Milburn, and T. M. Stace, in *Superconducting Devices in Quantum Optics*, edited by R. H. Hadfield and G. Johansson (Springer International Publishing, Cham, Switzerland, 2016), pp. 139–162.
[8] A. Houck, D. Schuster, J. Gambetta, J. Schreier, B. Johnson, J. Chow, L. Frunzio, J. Majer, M. Devoret, S. Girvin, and R. Schoelkopf, Nature (London) **449**, 328 (2007).
[9] Y. Yin, Y. Chen, D. Sank, P. J. J. O'Malley, T. C. White, R. Barends, J. Kelly, E. Lucero, M. Mariantoni, A. Megrant, C. Neill, A. Vainsencher, J. Wenner, A. N. Korotkov, A. N. Cleland, and J. M. Martinis, Phys. Rev. Lett. **110**, 107001 (2013).
[10] M. Pechal, L. Huthmacher, C. Eichler, S. Zeytinoğlu, A. A. Abdumalikov Jr., S. Berger, A. Wallraff, and S. Filipp, Phys. Rev. X **4**, 041010 (2014).
[11] M. Pierre, I. Svensson, S. R. Sathyamoorthy, G. Johansson, and P. Delsing, Appl. Phys. Lett. **104**, 232604 (2014).
[12] J. Wenner, Y. Yin, Y. Chen, R. Barends, B. Chiaro, E. Jeffrey, J. Kelly, A. Megrant, J. Y. Mutus, C. Neill, P. J. J. O'Malley, P. Roushan, D. Sank, A. Vainsencher, T. C. White, A. N. Korotkov, A. N. Cleland, and J. M. Martinis, Phys. Rev. Lett. **112**, 210501 (2014).
[13] Z. H. Peng, S. E. de Graaf, J. S. Tsai, and O. V. Astafiev, Nat. Commun. **7**, 12588 (2016).
[14] M. P. da Silva, D. Bozyigit, A. Wallraff, and A. Blais, Phys. Rev. A **82**, 043804 (2010).
[15] C. Eichler, D. Bozyigit, C. Lang, L. Steffen, J. Fink, and A. Wallraff, Phys. Rev. Lett. **106**, 220503 (2011).
[16] F. Mallet, M. A. Castellanos-Beltran, H. S. Ku, S. Glancy, E. Knill, K. D. Irwin, G. C. Hilton, L. R. Vale, and K. W. Lehnert, Phys. Rev. Lett. **106**, 220502 (2011).
[17] C. Eichler, D. Bozyigit, and A. Wallraff, Phys. Rev. A **86**, 032106 (2012).
[18] D. Bozyigit, C. Lang, L. Steffen, J. M. Fink, C. Eichler, M. Baur, R. Bianchetti, P. J. Leek, S. Filipp, M. P. da Silva, A. Blais, and A. Wallraff, Nat. Phys. **7**, 154 (2011).
[19] I.-C. Hoi, T. Palomaki, J. Lindkvist, G. Johansson, P. Delsing, and C. M. Wilson, Phys. Rev. Lett. **108**, 263601 (2012).
[20] C. Lang, C. Eichler, L. Steffen, J. M. Fink, M. J. Woolley, A. Blais, and A. Wallraff, Nat. Phys. **9**, 345 (2013).
[21] C. Eichler, C. Lang, J. M. Fink, J. Govenius, S. Filipp, and A. Wallraff, Phys. Rev. Lett. **109**, 240501 (2012).
[22] C. Eichler, D. Bozyigit, C. Lang, M. Baur, L. Steffen, J. M. Fink, S. Filipp, and A. Wallraff, Phys. Rev. Lett. **107**, 113601 (2011).
[23] E. Zakka-Bajjani, F. Nguyen, M. Lee, L. R. Vale, R. W. Simmonds, and J. Aumentado, Nat. Phys. **7**, 599 (2011).
[24] E. Flurin, N. Roch, F. Mallet, M. H. Devoret, and B. Huard, Phys. Rev. Lett. **109**, 183901 (2012).
[25] E. P. Menzel, R. Di Candia, F. Deppe, P. Eder, L. Zhong, M. Ihmig, M. Haeberlein, A. Baust, E. Hoffmann, D. Ballester, K. Inomata, T. Yamamoto, Y. Nakamura, E. Solano, A. Marx, and R. Gross, Phys. Rev. Lett. **109**, 250502 (2012).
[26] Z. H. Peng, Y.-x. Liu, J. T. Peltonen, T. Yamamoto, J. S. Tsai, and O. Astafiev, Phys. Rev. Lett. **115**, 223603 (2015).
[27] P. Lähteenmäki, G. S. Paraoanu, J. Hassel, and P. J. Hakonen, Nat. Commun. **7**, 12548 (2016).
[28] S. J. Freedman and J. F. Clauser, Phys. Rev. Lett. **28**, 938 (1972).
[29] A. Aspect, P. Grangier, and G. Roger, Phys. Rev. Lett. **47**, 460 (1981).
[30] O. Benson, C. Santori, M. Pelton, and Y. Yamamoto, Phys. Rev. Lett. **84**, 2513 (2000).
[31] N. Akopian, N. H. Lindner, E. Poem, Y. Berlatzky, J. Avron, D. Gershoni, B. D. Gerardot, and P. M. Petroff, Phys. Rev. Lett. **96**, 130501 (2006).
[32] R. M. Stevenson, R. J. Young, P. Atkinson, K. Cooper, D. A. Ritchie, and A. J. Shields, Nature (London) **439**, 179 (2006).

[33] A. Dousse, J. Suffczynski, A. Beveratos, O. Krebs, A. Lemaitre, I. Sagnes, J. Bloch, P. Voisin, and P. Senellart, Nature (London) **466**, 217 (2010).
[34] M. Müller, S. Bounouar, K. D. Jons, M. Glassl, and P. Michler, Nat. Photonics **8**, 224 (2014).
[35] J. F. Clauser, Phys. Rev. D **9**, 853 (1974).
[36] R. Loudon, Rep. Prog. Phys. **43**, 913 (1980).
[37] A. Aspect, G. Roger, S. Reynaud, J. Dalibard, and C. Cohen-Tannoudji, Phys. Rev. Lett. **45**, 617 (1980).
[38] A. Ulhaq, S. Weiler, M. S. Ulrich, R. Roszbach, M. Jetter, and P. Michler, Nat. Photonics **6**, 238 (2012).
[39] C. Hamsen, K. N. Tolazzi, T. Wilk, and G. Rempe, Phys. Rev. Lett. **118**, 133604 (2017).
[40] S. R. Sathyamoorthy, A. Bengtsson, S. Bens, M. Simoen, P. Delsing, and G. Johansson, Phys. Rev. A **93**, 063823 (2016).
[41] J. Koch, T. M. Yu, J. Gambetta, A. A. Houck, D. I. Schuster, J. Majer, A. Blais, M. H. Devoret, S. M. Girvin, and R. J. Schoelkopf, Phys. Rev. A **76**, 042319 (2007).
[42] M. Pechal, J.-C. Besse, M. Mondal, M. Oppliger, S. Gasparinetti, and A. Wallraff, Phys. Rev. Applied **6**, 024009 (2016).
[43] C. Eichler, Y. Salathe, J. Mlynek, S. Schmidt, and A. Wallraff, Phys. Rev. Lett. **113**, 110502 (2014).
[44] K. Koshino, H. Terai, K. Inomata, T. Yamamoto, W. Qiu, Z. Wang, and Y. Nakamura, Phys. Rev. Lett. **110**, 263601 (2013).
[45] See Supplemental Material at http://link.aps.org/supplemental/10.1103/PhysRevLett.119.140504 for power autocorrelation measurements and additional information about the experimental setup, the data analysis, and the theoretical model. The Supplemental Material includes Refs. [46–48].
[46] C. Eichler, J. Mlynek, J. Butscher, P. Kurpiers, K. Hammerer, T. J. Osborne, and A. Wallraff, Phys. Rev. X **5**, 041044 (2015).
[47] C. Lang, Ph.D. thesis, ETH Zurich, 2014.
[48] H. J. Carmichael, *Statistical Methods in Quantum Optics 1: Master Equations and Fokker-Planck Equations*, 2nd ed. (Springer-Verlag, Berlin, 2002).
[49] D.-G. Welsch, W. Vogel, and T. Opatrny, Prog. Opt. **39**, 63 (1999).